Batteries & Supercaps

Research Article
doi.org/10.1002/batt.202300490

Chemistry Europe
European Chemical Societies Publishing

www.batteries-supercaps.org

Practical Evaluation of Anionic Redox in Li-rich Cathode: An Electrochemical Study

Haichuan Wu[+],[a] Linhui Zeng[+],[b] Yiming Zhang,[a] Lingling Wang,[a] Shiyu Luo,[c] Yuan Fang,[a] Yi Wu,[a] Yuteng Qu,[a] Huaijin Huang,[b] Suluo Li,[b] Baodan Zhang,*[a] Yu Qiao,*[a] and Shi-Gang Sun[a]

Lithium-rich (Li-rich) manganese-based layered oxide materials are promising candidates for positive electrode materials due to their high energy density. However, challenges such as transition metal cation migration and irreversible anionic redox hinder their application. This study employs various electrochemical methods to systematically investigate three types of cathode materials: $LiNi_{0.6}Mn_{0.2}Co_{0.2}O_2$ (NCM622), $Li_{1.12}Ni_{0.39}Mn_{0.49}O_2$ (Li1.12), and $Li_{1.2}Ni_{0.2}Mn_{0.6}O_2$ (Li1.2). The findings indicate that an increase in lithium content leads to higher participation of anions in Anion Redox Reactions (ARRs), resulting in an augmented capacity. However, this also brings about significant polarization. The activation process of Li-rich materials triggers the ARRs mechanism, resulting in a sharp increase in resistance. Voltage drops during shelving and cycling are closely tied to the ARRs occurring at high potentials in Li-rich materials. To make the best use of the additional capacity associated with ARRs, it is essential to adjust the formation/cycling voltage in accordance with the characteristics of positive electrode materials with varying lithium contents. This study offers valuable insights for the design and utilization of Li-rich materials.

Introduction

Li-rich manganese-based layered oxide materials have become a highly regarded candidate for cathode materials due to their high energy density.[1,2,3,4] However, in addition to the problems of interface and structural evolution, the migration of transition metal cations and the irreversible oxidation-reduction of oxygen anions also pose significant challenges to the application of Li-rich materials.[5]

Li-Rich materials have a typical layered O3 phase structure. Non-Li-rich layered oxides represented by NCM622 have a specific C2/m space group structure. In contrast, in Li-rich materials, layered oxide phases of the C2/m space group and Li-rich phases of the R-3 m space group coexist.[6] In this structure, compared with non-Li-rich layered positive electrode materials, the filling of Li ions in the transition metal ion layer of Li-Rich positive electrode materials makes Li-Rich materials have a Li–O–Li configuration, which allows them to undergo O-related Anion Redox Reactions (ARRs).[7,8] Although ARRs bring greater capacity than non-Li-rich layered oxides, in Li-rich materials, ARRs usually have poor reversibility and large kinetic hysteresis, which results in capacity loss and larger overpotential.[9,10,11] This leads to problems such as low first discharge efficiency, oxygen release during cycling, and poor rate performance. Many advanced characterizations (ssNMR; XAS; XRD) are focused on the reversibility of lithium and structural changes, but the reversibility and kinetics of ARRs lack corresponding characterization.[12,13,14]

Classical electrochemical testing is an often overlooked crucial in-situ characterization method.[12,15] In fact, applying various electrochemical characterizations to Li-rich materials can obtain rich kinetic-related information. For example, through constant current and constant voltage (CC-CV) mode, information about the oxidation-reduction behavior of materials under high pressure can be obtained. Especially for Li-rich materials, CC-CV mode can display information related to ARRs processes that occur in high-pressure areas; variable upper limit charging tests can reveal the charge compensation mechanism of oxidation-reduction reactions that occur at different charging stages during discharge; electrochemical impedance spectroscopy (EIS) and galvanostatic intermittent titration technique (GITT) are vital means to characterize the ion diffusion behavior and electrochemical reaction rate during the charging and discharging process of batteries. Through these two methods, the dynamic characteristics of Li-rich materials can be measured. These electrochemical characterizations allow us to delve deeper into the oxidation-reduction process in Li-rich materials and provide a deep comparison with non-Li-rich layered oxides represented by NCM622.

In this work, we use various electrochemical methods for research, including constant current charging (CC), constant

[a] H. Wu,[+] Y. Zhang, L. Wang, Y. Fang, Y. Wu, Y. Qu, B. Zhang, Y. Qiao, S.-G. Sun
State Key Laboratory of Physical Chemistry of Solid Surfaces, Collaborative Innovation Center of Chemistry for Energy Materials (iChEM), Department of Chemistry, College of Chemistry and Chemical Engineering, Xiamen University, Xiamen 361005, China
E-mail: zhangbaodan@stu.xmu.edu.cn
yuqiao@xmu.edu.cn

[b] L. Zeng,[+] H. Huang, S. Li
College of Energy, Xiamen University, Xiamen 361005, China

[c] S. Luo
College of Materials, Xiamen University, Xiamen 361005, China

[+] These authors contributed equally to this work.

Supporting information for this article is available on the WWW under https://doi.org/10.1002/batt.202300490

Research Article
doi.org/10.1002/batt.202300490
Chemistry Europe
European Chemical Societies Publishing

current and constant voltage (CC-CV), electrochemical impedance spectroscopy (EIS), constant current intermittent titration (GITT), etc.[16,17] We compared with non-ARRs' $LiNi_{0.6}Mn_{0.2}Co_{0.2}O_2$ (NCM622), commercial Li-rich material $Li_{1.12}Ni_{0.39}Mn_{0.49}O_2$ (Li1.12), and high Li-rich phase $Li_{1.2}Ni_{0.2}Mn_{0.6}O_2$ (Li1.2). The results of these experiments suggest that as the lithium content in Li-rich materials increases, the anions participating in Anion Redox Reactions (ARRs) increase, bringing greater additional capacity to the material, greater polarization, and more deteriorated diffusion coefficients and impedance. Based on this understanding, the necessity of adjusting the upper and lower cut-off voltages in the formation and application of Li-rich materials is emphasized. By adjusting the cut-off voltage, it is possible to fully stimulate and apply the additional capacity brought by ARRs while avoiding the harm of voltage loss and capacity loss caused by lingering at too high a voltage on Li-rich materials, achieving better capacity retention. At the same time, the hysteresis caused by ARRs and its kinetic properties are systematically displayed in electrochemistry.

Results and Discussion

NCM-622, Li1.12, and Li1.2 cathode materials were synthesized by high-temperature solid-state method, which was obtained by uniformly mixing the precursor with lithium source Li_2CO_3 in an agate mortar, then sintering and annealing in a muffle furnace. The morphology of NCM-622, Li1.12 and Li1.2 are observed from a scanning electron microscope (SEM), shown in Figure 1 a. All materials present ellipsoidal secondary particles formed by the accumulation of nanoscale small particles, which exhibit porous structures induced by carbon dioxide escape from carbonate. The typical high-nickel ternary cathode material NCM-622 has the largest size, whose diameter exceeds 10 μm observed from the image inserted in Figure 1 a and figure S1. The size characteristics of secondary particles in the high-nickel Li-rich material Li1.12 are similar to NCM-622 for better primary particle aggregation. Li1.2 appears to be an alternative in appearance compared to the previous two materials, with elongated primary particles and loose aggregation. That directly leads to the formation of secondary particles, also showing long strips and smaller sizes (around 4~10 μm).

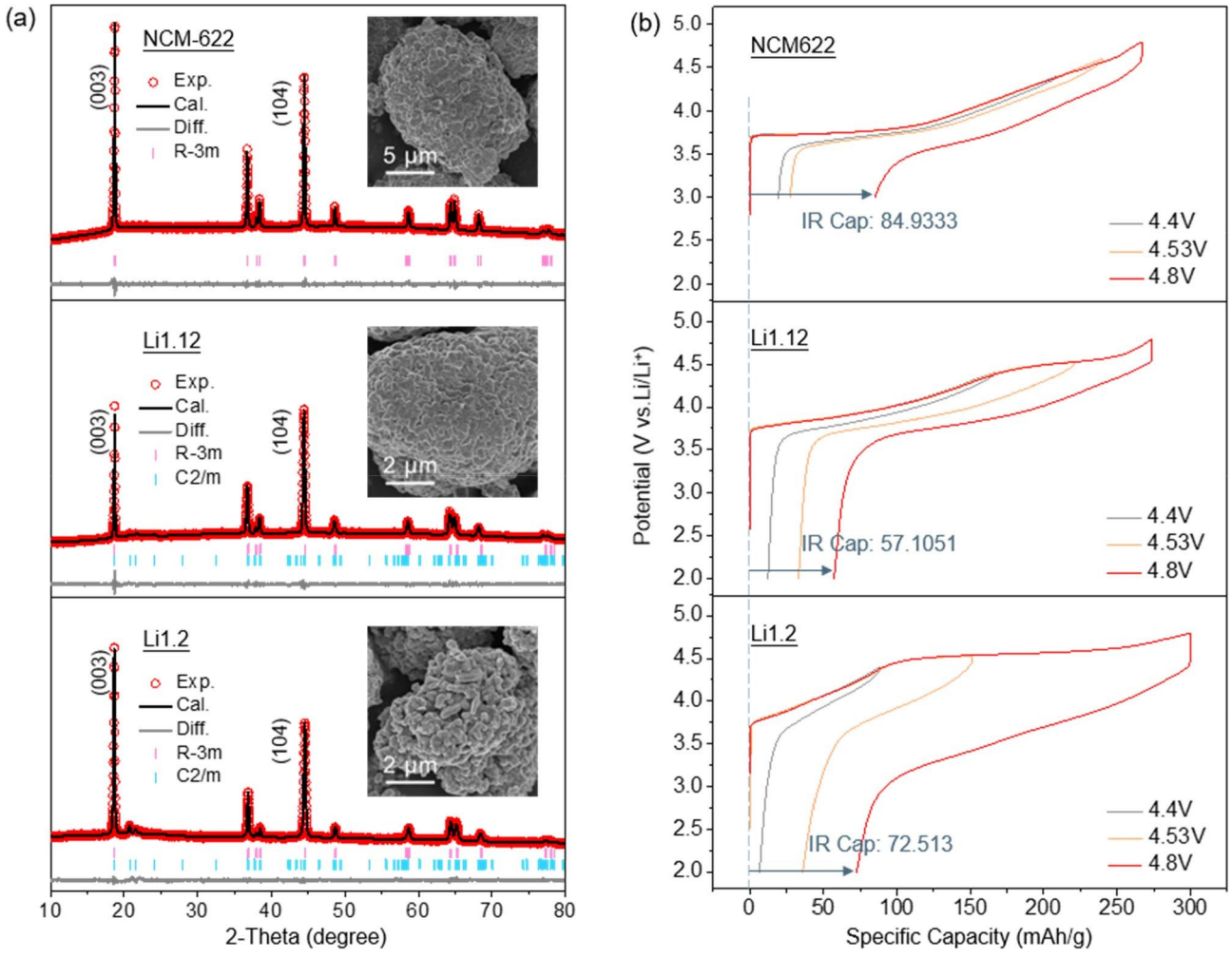

Figure 1. (a) XRD patterns of NCM622, Li1.12 and Li1.2 samples and the results of fitting via Rietveld refinement. Insert: corresponding SEM images. (b) Initial charge-discharge curves of NCM-622, Li1.12and Li1.2 at 0.05 C.

Research Article
doi.org/10.1002/batt.202300490
Chemistry Europe
European Chemical Societies Publishing

Powder X-ray diffraction (XRD) is introduced to investigate the crystalline differences of materials. Rietveld refinement result is calculated by GSAS, shown in Figure 1 a. The results show that the (003) peak of the high-nickel ternary cathode material is sharper and exhibits a more stable layered structure. The diffraction patterns for the other two materials show the structure that tends to be consistent with that of the Li-rich materials with hexagonal R-3 m and monoclinic C2/m space groups. The intensity ratio of (003) is relatively lower, appearing wider, indirectly indicating that the Li-rich structure has a certain degree of disorder. Besides, by carefully comparing the XRD patterns of the three, it can be found that compared with NCM-622, Li1.12 and Li1.2 exhibit superlattice diffraction peaks near 20.8°, corresponding to the existence of Li@Mn6 superstructure elements in the metal layer, which is the characteristic peak of the Li-rich phase (Li_2MnO_3).[18] The diffraction peak of Li1.2 with the highest lithium content is more significant in the range 20°~25°.[19]

The classical initial charge-discharge curves for three materials charged to 4.4 V, 4.53 V, and 4.8 V at a rate of 0.05 C and discharged to 2.0 V are shown in Figure 1 b. Generally, the slope below 4.5 V is mainly related to the oxidation of transition metal ions. In contrast, the potential plateau after 4.5 V represents the oxidation of lattice oxygen. With the increase in lithium content, Li-rich materials show a more extended high-voltage plateau, indicating an increase in anion activation. However, in NCM622, no high-voltage plateau is observed. The increase in lithium content also brings about a larger irreversible capacity, implying more irreversible anion redox. In NCM622, the irreversible polarization is higher than that of the two Li-rich materials, which may be due to the unusually high charging cut-off voltage causing irreversible structural collapse, and it lacks some anions with ARRs activity. It's worth noting that a more significant polarization is observed in Li1.2. With the increased lithium content, the amount of anions participating in anion redox reactions (ARRs) also increases, leading to weaker kinetics.[20,21]

To provide a more detailed examination of the electrochemical behavior, we conducted a series of tests on three cathode materials.[22] These materials were "activated" by gradually increasing the charging voltage window at a rate of 0.05 C and consistently discharging to 2.0 V. For NCM622, the charging window was progressively opened to 4.6 V. In contrast, the charging windows for Li1.12 and Li1.2 were expanded to 4.8 V. The resulting potential diagram, impedance diagram, and corresponding dQ/dV curves are presented in Figures 2 d, 2 e and 2 f.

Generally, cation oxidation can be nearly completed before reaching 4.2 V during the charging process. This suggests that any charging peaks observed above 4.2 V are primarily associated with anion oxidation. As depicted in Figure 2 d, for Li1.2, anion redox reactions occur at high voltage (>4.2 V) when the charging voltage exceeds 4.2 V. These reactions are reduced in the low voltage region (<3.5 V), leading to the emergence of two discharge peaks related to Anion Redox Reactions (ARRs). These peaks are indicated by arrows in the figure. Notably, Li1.2 exhibits a significant capacity for the

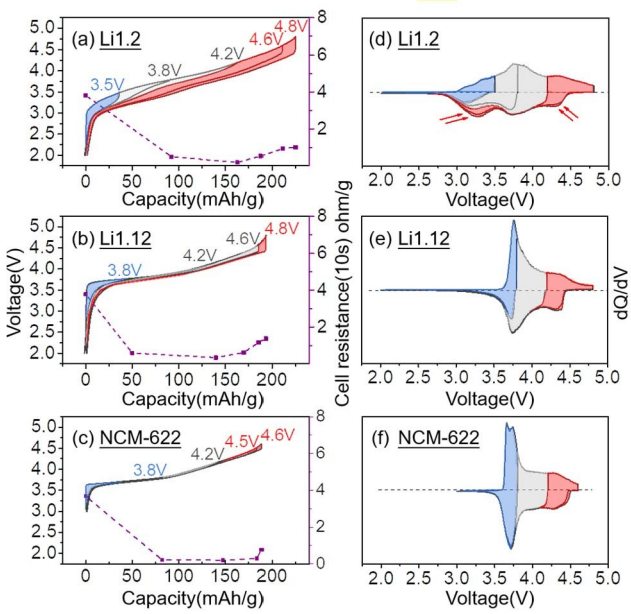

Figure 2. Voltage-capacity curves of (a) Li1.2, (b) Li1.12 and (c) NCM622. Corresponding dQ/dV chart of (d) Li1.2, (e) Li1.12 and (f) NCM622.

reduction in the low voltage region. However, as shown in Figures 2 e, f, almost no reduction in the low voltage region was observed for Li1.12 and NCM622. This indicates that Li1.2 has poorer kinetics, resulting in increased polarization. The degradation in kinetics becomes more severe as the content of the Li-rich phase increases. As the voltage window opens (as shown in Figures 2 d, e, f, the polarization resistance increases. This suggests that anion oxidation and reduction reactions contribute to an increase in polarization and a lag in voltage.[7]

To provide a more intuitive demonstration of the redox reaction kinetics during the discharge process, tests altering the discharge current density were conducted on three different materials.[23] NCM622 was charged to 4.6 V under a current density of 40 mA/g, and two Li-rich materials were charged to 4.8 V under the same current density. As Figure 3 depicts, Li1.2 exhibited greater polarization than Li1.12 when the current density was incrementally increased to 100 mA/g. For Li1.2, the peaks at both high (4.2 V) and low (3.2 V) potentials were primarily associated with anion oxidation and reduction, showing sensitivity to changes in current density. However, in the cases of NCM622 and Li1.12, no significant corresponding peaks for anion reduction at low potential were observed, which is consistent with previous discussions.

As the current density was further increased to 100 mA/g, the voltage drops of the corresponding discharge peaks were measured. These are presented in Figure 3 b. It was found that with an increase in the content of the Li-rich phase, the degree of polarization also increased. Specifically, the polarization of Li1.12 reached 0.0998 V, while that of Li1.2 reached 0.102 V, both higher than that of NCM622 (0.0896 V). This observation suggests that the capacity related to anion oxidation and reduction is more susceptible to the effects of electrochemical

Research Article
doi.org/10.1002/batt.202300490
Chemistry Europe
European Chemical Societies Publishing

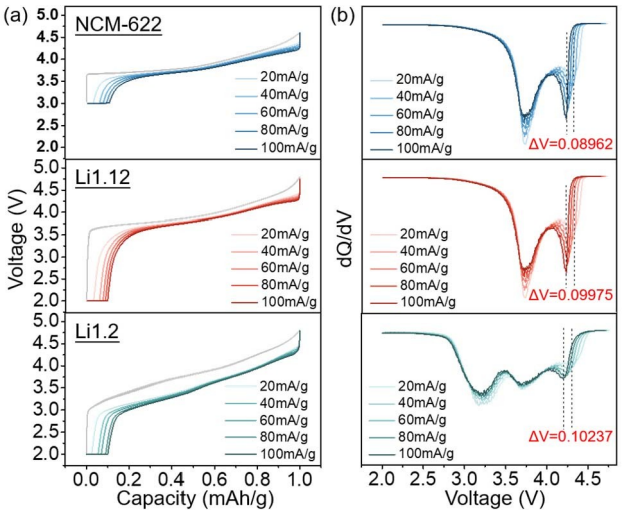

Figure 3. All cells are charged to upper limit voltage (4.6 V for NCM622 and 4.8 V for Li1.2 and Li1.12) at 40 mA/g and discharge at dif-current. The relevant curves are shown in (a) and corresponding dQ/dV charts of the discharging process are shown in (b).

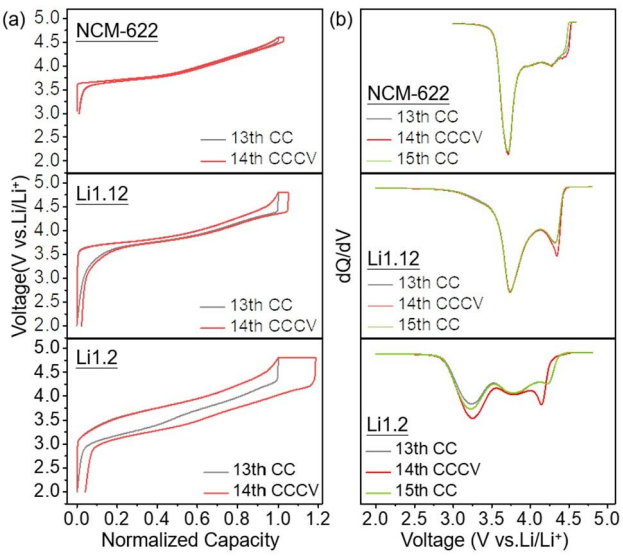

Figure 4. (a) Charge-discharge curves for the CC cycle (cycle 13) and CC-CV cycle (cycle 14) for NCM622, Li1.12 and Li1.2. (b) Discharge dQ/dV curve for NCM622, Li1.12 and Li1.2.

polarization. As such, the Li-rich phase content plays a crucial role in influencing this electrochemical behavior.

An assessment was conducted to examine the performance characteristics of three distinct materials under a constant current and constant voltage (CC-CV) charging protocol. This involved executing multiple cycles of constant current charge and discharge on batteries equipped with three types of cathodes until a stable cycle state was achieved.

The first material, NCM622, underwent cycling within a voltage range of 3.0–4.6 V. The other two materials, Li1.12 and Li1.2, were cycled within a broader voltage range of 2.0–4.8 V. Following these cycles, each material continued with constant voltage charging at their respective charging cut-off voltages in the subsequent charge and discharge cycle (as shown in Figure 4 a). After the CC-CV cycle, constant current charge and discharge were resumed. The discharge dQ/dV curves for the CC-CV cycle (cycle 14), its preceding constant current charge and discharge cycle (cycle 13), and the subsequent constant current charge and discharge cycle (cycle 15) are depicted in Figure 4. Figure 4 b illustrates that the discharge dQ/dV curve for NCM622's cycle 15 underwent severe structural distortion. This could be attributed to significant structural damage within NCM622 caused by high voltage constant voltage charging. However, Figure 4 b also reveals that the discharge dQ/dV curve for cycle 15 of Li1.12 did not exhibit any noticeable shape changes compared to the discharge dQ/dV curve of its cycle 13. Interestingly, Li1.2 generated more capacity during the constant voltage charging stage. In cycle 15, Li1.2 exhibits more capacity related to anion oxidation and reduction at low potential during the constant voltage stage. These observations suggest that constant current charging at a high voltage of 4.8 V did not result in apparent irreversible capacity loss to Li-rich materials. In Li-rich materials with a high lithium content, like Li1.2, there is still capacity related to anion redox reactions (ARRs) in the bulk phase that cannot be fully activated. This capacity can be stimulated under a constant voltage charge. The high-voltage CV plateau would cost more time than the typical CC mode, it may be meaningless for NCM622 while helpful for Li-rich materials, especially for Li1.2. However, more detailed research is still needed to balance the trade-off between time cost and capacity improvement because the capacity improvement of Li1.12 is less significant than Li1.2.

Two electrochemical techniques, EIS and GITT, have been used to characterize interface kinetic and internal diffusion.[15,24] The overall trend of the Nyquist spectra of the three materials is roughly as follows. At the beginning of the charge, the Nyquist plot of EIS shows the diffusion and migration of Li-ion through the surface insulation layer of the active material particles, which is related to the fast electrochemical processes of the high frequencies (HF) semicircle. Throughout the charging process, the first relaxation exhibits the highest HF resistance (Figure 5 b, f, j), while the remaining HF resistances remain the same in size in the subsequent process. In the medium frequencies (MF) region, the semicircle shown in the EIS Nyquist plot is related to the interfacial charge-transfer resistance (R_{ct}). Initially, the arc associated with R_{ct} is sizeable, while it gradually decreases as charging processes and remains almost stable until the end of charging. The semicircle related to R_{ct} rapidly expands until the end of charging, indicating that the charge-transfer resistance is relatively low and steady during the primary charging process, which means fast charge-transfer kinetics. A valley is shown on the trends for variations of R_{ct} vs. SOC (Figure 5 a, e, i).

Among the three kinds of cathode electrode materials, NCM622 exhibits the most stable R_{ct}, with the most minor changes in the charging process. For the other two Li-rich cathode materials, the situation is significantly worse. Due to the unique anionic oxidation-reduction process of Li-rich cathode materials, the kinetic process of charge transfer

Research Article
doi.org/10.1002/batt.202300490
Chemistry Europe
European Chemical Societies Publishing

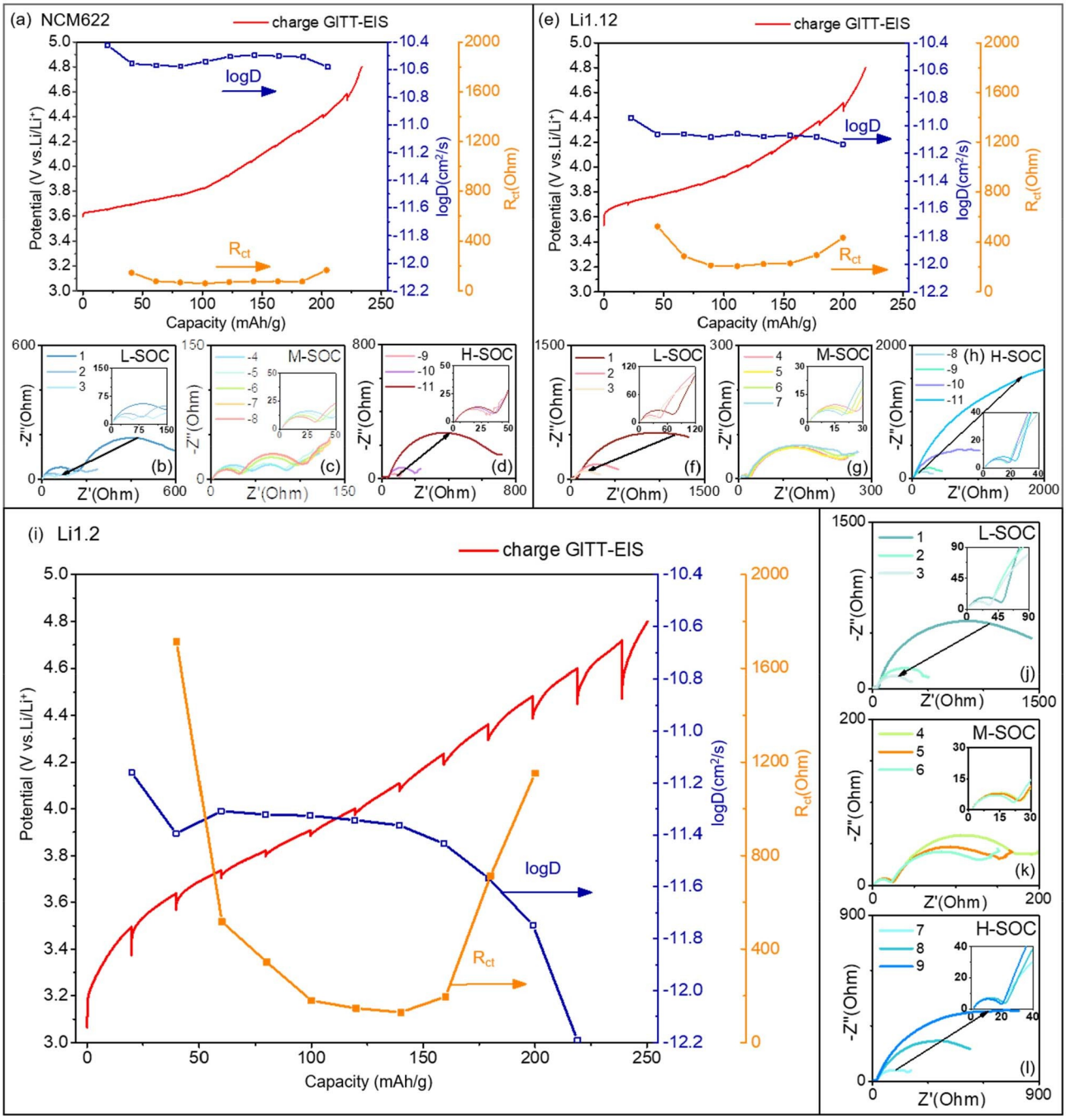

Figure 5. EIS-GITT profiles for charge in 3-electrode cells for (a) NCM622, (e) Li1.12 and (i) Li1.2. Nyquist spectra for NCM622 on charge are shown for low-SOC in (b), mid-SOC in (c) and high-SOC in (d). Similarly, for Li1.12 and Li1.2, for low-SOC in (f) and (j), mid-SOC in (g) and (h) and high-SOC in (k) and (l).

substantially deteriorates. With the increase of Li-rich content (intensification of anionic oxidation-reduction), the overall R_{ct} also continuously increases. This phenomenon is manifested as a significant increase in the R_{ct}-SOC curve in the second half of SOC.

The diffusion coefficient of lithium-ion is characterized by calculating the value of logD (Figure 5 a, e, i and Figure S2). During the whole charging process, for NCM622, the value of logD fluctuates around a relatively stable and low value (approximately -10.5 cm^2/s), while the logD of Li1.12 may be slightly smaller, but it still fluctuates around the value (about -11.05 cm^2/s). The diffusion coefficient of Li1.2 rapidly decreases near the end of charging, indicating that profound anion redox reaction significantly impacts the Li-ion diffusion process. The value of logD dropped directly from -11.3 cm^2/s to -12.2 cm^2/s, which the diffusion coefficient decreased by an order of magnitude. The above results indicate that as the lithium content increases, the diffusion coefficient decreases and the impedance increases, showing more deteriorated kinetic characteristics.

An ageing experiment was carried out over a span of 36 hours, with temperature being the variable under consideration. The experiment was conducted under two distinct temperature conditions: ambient room temperature and an elevated temperature of 55 °C.[25] Observations were made on the dQ/dV profiles at a rate of 0.05 C, both prior to and following the ageing process. These observations are illustrated in Figure 6. This indicates that at high temperatures, the loss of Ni in NCM622 and Li^+/Ni^{2+} cation mixing lead to structural changes and increased polarization.[26] Li1.2 demonstrated commendable stability at high voltages at room temperature after the 36-hour ageing period. In Li-rich materials, high temperatures activate anions, improving kinetics, causing a larger curve change in Li1.2, and reducing polarization.[27] In contrast, when subjected to a higher temperature of 55 °C, NCM622 displayed more consistent changes in its redox pair. It was noted that the redox pair remained stable even after 36 hours of ageing. However, Li1.12 and Li1.2 showed significant shifts in their redox pairs during the high-temperature ageing process. Notably, the shift in Li1.2 was more pronounced than in Li1.12, indicating that elevated temperatures accelerate the ageing process of the Li-rich cathode. The most substantial voltage offset for the Li-rich cathode occurred at high potentials associated with anionic redox reactions. This suggests that the voltage loss resulting from ageing is linked to anionic redox reactions occurring in Li-rich materials at high potentials during the ageing process. O-related anionic redox would be stimulated under the higher temperature. As the concentration of the Li-rich phase increases, this situation exacerbates and exhibits a markedly stronger sensitivity to temperature variations.

Long cycle tests (under 0.05 C) were conducted under different conditions for three types of cathode materials to compare the effects of varying activation and cycling strategies on cathode materials.[28,29] The changes in discharge-specific capacity with the number of cycles during the test are shown in Figure 7. As shown in Figure 7 a, NCM622 shows significant capacity decay when cycled at higher charge cut-off voltages (4.5–4.6 V), caused by structural distortion in the high voltage range.

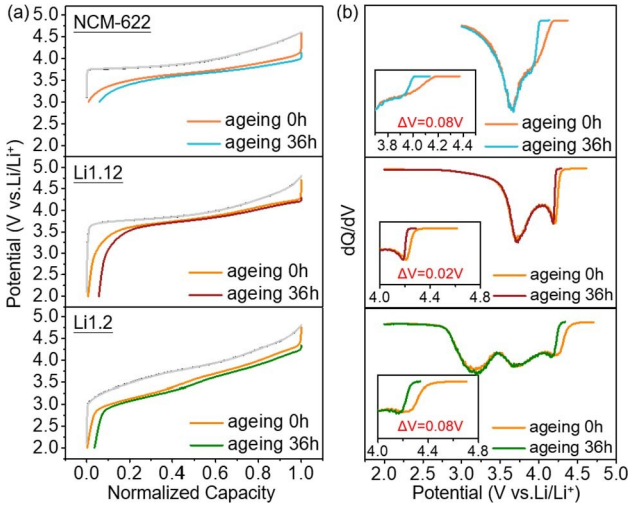

Figure 6. (a) Charge-discharge curves and dQ/dV profiles for NCM622, Li1.12 and Li1.2 at a rate of 0.05 C after 0-hour and 36-hour ageing (at 55 °C) period.

Lowering the cycling voltage of NCM622 to 3–4.5 V can improve the cycle stability of NCM622, but raising the activation voltage of NCM622 from 3–4.5 V to 3–4.6 V cannot obtain more specific capacity. As shown in Figure 7 b, in Li1.12, the discharge-specific capacity obtained from 2–4.8 V formate 2–4.6 V cycling is close to that obtained from 2–4.8 V formate 2–4.8 V cycling in the early cycles. It shows a better capacity retention rate until the 250th cycle. After activation at higher voltages (2–4.8 V), if a higher charge cut-off voltage is used for cycling, the Li-Rich cathode may stay in the high voltage area for too long, causing large polarization and excessive irreversible ARRs, accelerating capacity decay. After high-voltage activation, adopting a relatively lower cycling charge cut-off voltage can obtain significantly better capacity retention while obtaining similar discharge capacity. However, after lowering the formation voltage to 2–4.7 V formate 2–4.6 V cycling, although a gradual excitation of capacity is observed during cycling, both capacity and retention rate are worse than those of 2–4.8 V formation. The Li1.2 with higher lithium content (Figure 7 c) shows higher discharge specific energy than 2–4.8 V formate 2–4.6 V cycling in the first 200 cycles under higher formation voltage (2–4.8 V) and higher charge cut-off voltage (2–4.8 V), and the capacity is gradually excited during cycling. The cathode of 2–4.7 V formate 2–4.6 V cycling has slightly less capacity than that of 2–4.8 V formate 2–4.6 V cycling in the early cycles. Still, it shows significantly less capacity decay when cycled to 200 cycles, indicating that for Li1.2, a formation voltage lower than 4.8 V may be more reasonable. The above results show that for rational use of ARRs related to extra capacity, it is necessary to adjust the formation/cycling voltage according to the characteristics of cathode materials with different lithium contents.

Figures 7 d, f present a comparison of the changes in discharge-specific capacity with the cycle number under high temperatures (55 °C) for two types of Li-Rich materials. These materials were tested under two different cycling conditions: 2–4.6 V formate 2–4.6 V cycling and 2–4.7 V formate 2–4.6 V cycling. The results indicate that the high-temperature activation strategy does not significantly increase the capacity compared to room-temperature activation. Furthermore, high-temperature activation greatly accelerates the capacity decay of the Li-rich cathode. This suggests that high-temperature activation may not be suitable for Li-rich cathodes.

Conclusions

In this study, we used a variety of electrochemical methods (variable upper limit charging, cha-discharge, CC-CV, GITT, EIS, shelving, long cycle, etc.) to systematically study three types of cathode materials: NCM622, Li1.12, and Li1.2. We obtained the following conclusions:

Research Article
doi.org/10.1002/batt.202300490
Chemistry Europe
European Chemical Societies Publishing

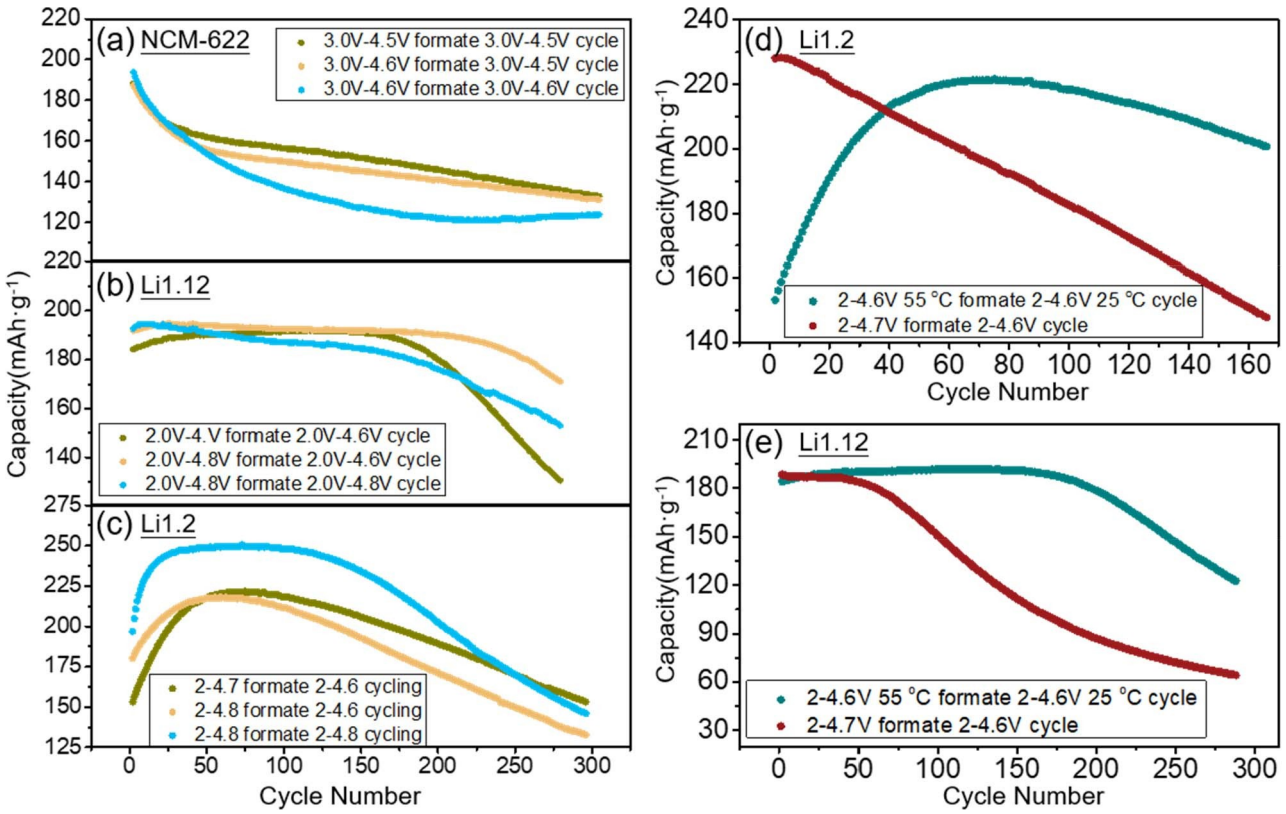

Figure 7. Cycling performances (discharge capacity vs. cycle number) of (a) NCM622, (b) Li1.12 and (c) Li1.2 within 300 cycles which activated at room temperature but at different voltage. The same cycling performances comparison of (d) Li1.2 and (e) Li1.12 which activated at 55 °C at the voltage of 2–4.6 V and activated at room temperature at the voltage of 2–4.7 V.

(1) With the increase in lithium content, the number of anions participating in ARRs will also increase. While bringing additional capacity, it also leads to a more severe polarization increase and voltage lag. The capacity related to ARRs is more susceptible to electrochemical polarization.
(2) The ARRs mechanism triggered by the activation process of Li-rich materials leads to a sharp increase in resistance, whether from the perspective of charge transfer impedance or diffusion coefficient.
(3) The voltage loss in shelving and cycling is related to the ARRs at high potentials in Li-rich materials. To make rational use of the ARRs related to additional capacity, it is necessary to adjust the formation/cycling voltage according to the characteristics of the positive electrode materials with different lithium contents. In addition, the strategy of high-temperature activation is unsuitable for Li-rich materials.

The electrochemical tests have clarified the interaction between ARRs and kinetics. We hope this can provide electrochemical guidance for designing and applying Li-rich materials.

Author Contributions

H. W and L. Z. contributed to the design of the research and performed the experimental data analysis. H. W., L. W and Y. Z. contributed to electrochemical tests. L. Z., L. W. and Y. Z. performed GITT and EIS tests. Y. Z. conducted SEM and XRD characterization. Y. F., S. L., Y. W., S. L., H. H. and Y. Q. contributed to the writing of the article and assisted with the experiment. B. Z., Y. Q. and S. S. supervised the work. All authors discussed the results, co-wrote and commented on the manuscript. H. W. and L. Z. contributed equally to this work.

Acknowledgements

This work was partially supported by Open Innovation Fund for Precious Experimental Instruments and Equipment for Top Students of Xiamen University: Design and characterization of material systems related to lithium-ion batteries (grant no. KFJJ-202203), College Student Innovation Training: Structural Research and Performance Regulation of Lithium-rich Cathode Materials for Lithium-ion Batteries (project no. 2022X1232). This paper has used AI tools such as ChatGPT for language and text processing unrelated to scientific results. This is hereby declared and acknowledged.

Conflict of Interests

The authors declare no competing financial interests.

Data Availability Statement

The data that support the findings of this study are available from the corresponding author upon reasonable request.

Keywords: Lithium-rich manganese-based layered oxide materials · Anion Redox Reactions (ARRs) · Electrochemical polarization · Impedance · Voltage loss

[1] S. Liu, B. Wang, X. Zhang, S. Zhao, Z. Zhang, H. Yu, *Matter* **2021**, *4*, 1511–1527.
[2] T. Lin, T. Seaby, Y. Hu, S. Ding, Y. Liu, B. Luo, L. Wang, *Electrochem. Energy Rev.* **2022**, *5*, 27.
[3] X. Q.-J. Z. Luo-Zeng, T. Wei-Ping, J. Xue, Y. Xiao-Lei, *J. Electrochem.* **2015**, *21*, 138–144.
[4] X. Cao, H. Li, Y. Qiao, M. Jia, H. Kitaura, J. Zhang, P. He, J. Cabana, H. Zhou, *Sci Bull (Beijing)* **2022**, *67*, 381–388.
[5] W. E. Gent, K. Lim, Y. Liang, Q. Li, T. Barnes, S. J. Ahn, K. H. Stone, M. McIntire, J. Hong, J. H. Song, Y. Li, A. Mehta, S. Ermon, T. Tyliszczak, D. Kilcoyne, D. Vine, J. H. Park, S. K. Doo, M. F. Toney, W. Yang, D. Prendergast, W. C. Chueh, *Nat. Commun.* **2017**, *8*, 2091.
[6] B. Zhang, Y. Zhang, H. Wu, L. Zeng, X. Wang, H. Liu, X. Wu, J. Chen, H. Zhang, Y. Yan, Y. Tang, H. Huang, L. Zheng, Q. Zhang, Q. Xie, D.-L. Peng, C. Li, Y. Qiao, S.-G. Sun, *Energy Storage Mater.* **2023**, *62*, 102926.
[7] G. Assat, J. M. Tarascon, *Nat. Energy* **2018**, *3*, 373–386.
[8] M. Oishi, C. Yogi, I. Watanabe, T. Ohta, Y. Orikasa, Y. Uchimoto, Z. Ogumi, *J. Power Sources.* **2015**, *276*, 89–94.
[9] Liu, Haodong, Zhang, Minghao, Hy, Sunny, Hwang, Bing-Joe, Qian, Danna, *Energy & Environmental Science Ees* **2016**, *9*, 1931–1954.
[10] A. Manthiram, J. C. Knight, S. T. Myung, S. M. Oh, Y. K. Sun, *Advanced Energy Materials* **2016**, *6*, 1501010.
[11] D. Luo, H. Xie, F. Tan, X. Ding, J. Cui, X. Xie, C. Liu, Z. Lin, *Angew. Chem. Int. Ed. Engl.* **2022**, *61*, e202203698.
[12] B. Zhang, Y. Zhang, X. Wang, H. Liu, Y. Yan, S. Zhou, Y. Tang, G. Zeng, X. Wu, H. G. Liao, Y. Qiu, H. Huang, L. Zheng, J. Xu, W. Yin, Z. Huang, Y. Xiao, Q. Xie, D. L. Peng, C. Li, Y. Qiao, S. G. Sun, *J. Am. Chem. Soc.* **2023**, *145*, 8700–8713.
[13] R. A. House, G. J. Rees, M. A. Pérez-Osorio, J. J. Marie, P. G. Bruce, *Nature Energy* **2020**, *5*, 777–785.
[14] H. Zhang, H. Liu, L. F. J. Piper, M. S. Whittingham, G. Zhou, *Chem. Rev.* **2022**, *122*, 5641–5681.
[15] G. Assat, C. Delacourt, D. A. D. Corte, J.-M. Tarascon, *J. Electrochem. Soc.* **2016**, *163*, A2965–A2976.
[16] J. Wang, H. Liu, C. Du, B. Liu, H. Guan, Y. Liu, S. Guan, Z. Sun, H. Yao, *eScience* **2023**, 100224.
[17] W. Guo, W. Wei, H. Zhu, Y. Hu, H. Jiang, C. Li, *eScience* **2023**, *3*, 100082.
[18] Y. Yang, H. Su, T. Wu, Y. Jiang, D. Liu, P. Yan, H. Tian, H. Yu, *Sci Bull (Beijing)* **2019**, *64*, 553–561.
[19] R. Shunmugasundaram, R. S. Arumugam, J. R. Dahn, *J. Electrochem. Soc.* **2016**, *163*, A1394–A1400.
[20] H. Yu, Y. G. So, A. Kuwabara, E. Tochigi, Y. Ikuhara, *Nano Letters* **2016**, *16* (5), 2907–2915.
[21] C.-G. S. Chen-Xu Luo, Zhi-Yuan Yu, Ling Huang, Shi-Gang Sun, *J. Electrochem.* **2022**, *28*, 2006131.
[22] G. Assat, D. Foix, C. Delacourt, A. Iadecola, R. Dedryvère, J.-M. Tarascon, *Nat. Commun.* **2017**, *8*, 2219.
[23] Y. Wang, Z. Yang, Y. Qian, L. Gu, H. Zhou, *Adv. Mater.* **2015**, *27*, 3915–3920.
[24] M. Guo, R. E. White, *J. Power Sources* **2012**, *198*, 322–328.
[25] T. Ohzuku, M. Nagayama, K. Tsuji, K. Ariyoshi, *J. Mater. Chem.* **2011**, *21*, 10179–10188.
[26] S. Liu, J. Su, J. Zhao, X. Chen, C. Zhang, T. Huang, J. Wu, A. Yu, *J. Power Sources* **2018**, *393*, 92–98.
[27] H. Yu, Y. G. So, Y. Ren, T. Wu, G. Guo, R. Xiao, J. Lu, H. Li, Y. Yang, H. Zhou, *J. Am. Chem. Soc.* **2018**, *140*, 15279–15289.
[28] R. Väli, S. Aftanas, A. Eldesoky, A. Liu, T. Taskovic, J. E. Harlow, J. deGooyer, N. Phattharasupakun, D. Ouyang, D. Rathore, M. M. E. Cormier, M. B. Johnson, H. Nguyen, H. Kwak, S. Kumakura, J. Paulsen, J. R. Dahn, *Journal of The Electrochemical Society* **2022**, *169*, 060530.
[29] R. Yu, C. Wang, H. Duan, M. Jiang, A. Zhang, A. Fraser, J. Zuo, Y. Wu, Y. Sun, Y. Zhao, J. Liang, J. Fu, S. Deng, Z. Ren, G. Li, H. Huang, R. Li, N. Chen, J. Wang, X. Li, C. V. Singh, X. Sun, *Adv. Mater.* **2023**, *35*, e2207234.

Manuscript received: October 19, 2023
Revised manuscript received: December 26, 2023
Accepted manuscript online: December 27, 2023
Version of record online: January 12, 2024